# Evaluating the Vulnerability of *Tetracentron sinense* Habitats to Climate-Induced Altitudinal Shifts

Yuanjie Gan[1], Lijun Chen[1], Junfeng Tang[1], Yan Han[1], and Xiaohong Gan[1]

[1]China West Normal University

July 28, 2024

**Abstract**

**Objective:** Exploring the evolving geographical distribution pattern of *Tetracentron sinense* and its main influencing factors since the last interglacial can provide a scientific foundation for the efficient conservation and administration of the species. **Methods:** The MaxEnt model was used to construct the potential distribution areas of *T. sinense* in different periods such as the last interglacial, the last glacial maximum, the Mid-Holocene, the current and future. On the premise of discussing the influence of dominant environmental factors on its distribution model, the suitable area changes of *T. sinense* under different ecological climate situations were quantitatively analyzed. **Results:** The AUC value predicted by the optimized model was 0.959, indicating a good predictive effect by the MaxEnt model; the potential suitable areas for *T. sinense* in the current are mainly located in southwest China, which are wider compared to the actual habitats. Jackknife testing showed that the lowest temperature in the coldest month, elevation, seasonal variation coefficient of temperature and surface calcium carbonate content are the dominant environmental factors affecting the distribution of *T. sinense*. From the last interglacial to the current, the total suitable area of *T. sinense* showed a decreasing trend; the distribution points of *T. sinense* populations in Mid-Holocene may be the origin of the postglacial population, and Southwest China may be its glacial biological refuge. Compared with the current, the total suitable area ranges of *T. sinense* in China in the future decreased, and the centroid location of its total fitness area all migrated to the northwest, with the largest migration distance in 2070s under the SSPs 7.0 climate scenario. **Conclusion:** Temperature was the most important factor affecting the distribution of *T. sinense*. With the global warming, its suitable area ranges will show a shrinking trend. Ex-situ conservation measures could be taken to preserve its germplasm resources.

## 1 Introduction

The geographical distribution of plant populations is influenced by both the biological characteristics of the plant species and their environment (Thuiller et al., 2005; Ge et al., 2012). Primarily, the climate within large-scale regions serves as the principal determinant affecting species distribution. Changes in climate consequently alter species' responses and selection to climate and habitat (Ma et al., 2022). In recent times, exacerbated by climate change and human interference, species habitats have suffered severe degradation. This degradation is particularly notable in the significant reduction of suitable growth areas for endangered plants, leading to diminished resources for wild species (Lenoir et al., 2008; Liu et al., 2015). Consequently, investigating the impacts of changing climates on species distribution patterns is crucial for understanding historical and future changes in species range and can furnish a scientific foundation for conserving germplasm resources in endangered plants (Li et al., 2021).

Species distribution models (SDMs) rely on various environmental variables such as climate and soil, closely related to the real growth and distribution of species. These models can predict potential suitable distribution areas of species using specific algorithms, thereby elucidating the predominant environmental factors influencing their distribution and exploring the ecological requirements of species (Araújo et al., 2012). Among the myriad of models, SDMs encompass 19 different methodologies, including the rule-set genetic algorithm model (GARP), maximum entropy model (MaxEnt), and ecological factor analysis models (ENFA) (Phillips et al., 2008). The MaxEnt model stands out due to its relative maturity, ease of operation, and high prediction accuracy (Hao et al., 2020). It can infer and predict from incomplete known information, making it widely applicable in studying the introduction and cultivation of relict plants, horticultural tree species, and invasive plants (Elith et al., 2006).

*Tetracentron sinense* Oliv., a Tertiary relict plant, represents the sole surviving species in the *Tetracentron* genus of the Trochodendraceae family (Fan et al., 2021). This species holds significant importance in the discussion of the systematic evolution of angiosperm plants. Unfortunately, due to its ornamental, furniture, and medicinal value, *T. sinense* has been subjected to extensive exploitation by humans, resulting in poor regeneration of its natural populations (Pang et al., 2018; Lu et al., 2020; Wang et al., 2023). Consequently, it has been designated as a national secondary protection plant in China and listed in Appendix III of the Convention on International Trade of Endangered Species (Fu, 1992). The preservation of germplasm resources has garnered considerable attention from researchers (Duan et al., 2019; Zhang et al., 2019).

Fossil records indicate that *Tetracentron* Oliv. was once widely distributed across Europe, North America, and East Asia during the Pleistocene era (Rix, 2007). A phylogeographical analysis based on the chloroplast genome suggests that the current geographical distribution pattern of *T. sinense* may have been shaped by Quaternary climate oscillations, with Southwest China potentially serving as a biological refuge during glacial periods (Sun et al., 2014). Li et al. (2018) observed a correlation between the phenotypic variation of *T. sinense* and environmental factors such as mean annual sunshine duration, mean temperature in July, and annual mean precipitation. However, the specific influence of these environmental factors on the geographic distribution of *T. sinense* remains ambiguous. Additionally, how will the distribution pattern of *T. sinense* evolve in the context of past and future climate changes? What are the primary environmental factors constraining its geographical distribution? And how do these factors influence its distribution? These questions remain unanswered, impeding the effective protection and management of *T. sinense* germplasm resources.

Utilizing the MaxEnt model and ArcGIS spatial analysis technology, this study examines potentially suitable areas for *T. sinense* across historical periods (the last interglacial period, the last glacial maximum, and the Middle Holocene) as well as current and future periods (2050s and 2070s). The objectives of this study are to (1) analyze the dynamic changes in potentially suitable areas, (2) investigate the main environmental factors driving changes in the distribution pattern of *T. sinense* , and (3) furnish a scientific basis for the effective protection and management of *T. sinense* .

## 2 Materials and Methods

### *2.1 Data Collection and Preprocessing of Distribution Point Data*

A total of 199 distribution records of *T. sinense* were sourced from various data platforms, including Flora Reipublicae Popularis Sinicae (http://iplant.cn/), Plant Photo Bank of China, and the Global Biodiversity Information Facility (GBIF, http://www.gbif.org). Additionally, our research group conducted field investigations, yielding 121 distribution data points. Consequently, a comprehensive dataset comprising 320 distribution records of *T. sinense* was compiled.

The coordinate points of *T. sinense* , denoted by latitude and longitude, were converted into decimal numbers compatible with ARCGIS using standard formulas. The resulting table contained three columns: space, longitude, and latitude, and was stored in CSV format. Subsequently, the distribution data in CSV format were imported into ARCGIS 10.2. By utilizing the "Data/Display XY data" and "Data/Export data" functions, a vector file representing the distribution points of *T. sinense* was generated. The projection utilized the WGS1984 geographic coordinate system, with each grid layer retaining only one distribution point. This process ensured an accuracy of 2.5 m, facilitated by ENMTTools software. Following the removal of duplicate entries and the mitigation of sampling deviations, a final set of 232 distribution points was selected (Fig. 1).

### *2.2 Environmental Variables*

We gathered environmental variables associated with bioclimatic, soil, and topographic factors as potential predictors of species distribution (Table 1). 19 climate variables spanning the last glacial, last glacial maximum, Mid-Holocene, current periods, and future scenarios were sourced from the World Climate Database (http://worldclim.org) (Gao et al., 2018). Future scenarios included low-concentration emissions (SSPs1-2.6) and high-concentration emissions (SSPs5-8.5) of greenhouse gases. 16 soil variables pertaining to the soil surface were acquired from the Chinese Soil Dataset within the Harmonized World Soil Database (HWSD, http://www.fao.org/faostat/en/#data), while elevation data were obtained from the same source. The spatial resolution was set at 2.5 m. Map data were represented in SHP format based on a 1:1 million scale Chinese map obtained from the National Center for Basic Geographic Information.

To mitigate multicollinearity and potential model overfitting (Graham, 2003), we conducted Spearman's correlation analysis within ArcGIS (Yang et al., 2013) to examine relationships among environmental factors. Variables demonstrating a correlation coefficient of [?] 0.8 were considered highly correlated, and the less influential factor was excluded from subsequent analysis. Consequently, a total of 16 environmental factors were retained for calculation and analysis within the MaxEnt model.

Climate and elevation variable data were clipped according to the vectograph of a 1:1 million scale Chinese administrative map and then converted to ASC format using ArcGIS software. Soil variable data were integrated by importing the China soil file and HWSD DATA file into ArcGIS software. Subsequently, the grid layer comprising the 16 soil variables within the MU_GLOBAL layer was extracted and converted into ASC format. Finally, all environmental variable layers underwent batch processing using ArcGIS software, resulting in environment layers with non-overlapping extents.

*2.3 Model Building, Optimization, and Evaluation*

In accordance with the latest model optimization methodology proposed by Cobos et al. (2019), adjustments were made to the parameters of the MaxEnt model to assess the degree of alignment between the distribution points of *T. sinense* and the model, as determined by the corrected Akaike information criterion (AICc) (Yu et al., 2019). Optimal model parameters, indicated by the lowest AICc value, were selected for utilization within the MaxEnt software (Philips et al., 2017).

The distribution data of *T. sinense* and its corresponding environmental variables spanning the study period were inputted into the MaxEnt model. In this investigation, 25% of the 232 distribution sites of *T. sinense* were earmarked for model evaluation, while the remaining 75% constituted the training set for constructing a response curve. 10 replicates were generated for each training partition, and the resultant outcomes were averaged. Model results were generated in both Logistic and ASC format files, with a multi-feature combination based on optimization outcomes (Moreno et al., 2011).

To calibrate the model and verify its robustness, the receiver operating characteristic (ROC) curve was analyzed, independent of the threshold. The area under the curve (AUC) was computed to ascertain the accuracy of the model. Model performance was categorized as failure (0.5-0.6), poor (0.6-0.7), fair (0.7-0.8), good (0.8-0.9), or excellent (0.9-1.0), with higher AUC values indicating superior model performance (Fithian et al., 2015).

*Classification of Fitness Levels and Area Statistics*

The average output data from each period, following 10 simulations in the MaxEnt model, were imported into ArcGIS software. These data were then converted into raster layers and subsequently reclassified based on the distributed probability (P) values. Employing natural breakpoint classification, the distribution area of *T. sinense* was categorized into four distinct levels: Non-suitable area ($P < 0.2$), Low suitable zone (0.2 [?] $P < 0.4$), Intermediate suitable zone (0.4 [?] $P < 0.6$), High suitable zone (P [?] 0.6) The reclassified layers were processed using an ArcGIS grid table to determine the area encompassed by each level (Zhuang et al., 2018).

*2.5 Screening and Threshold Analysis of Dominant Climate Factors*

We conducted an **analysis** to identify the primary environmental factors influencing the distribution of *T. sinense* . This analysis relied on assessing the permutation importance (PI) and permutation contribution (PC) of environmental variables within the prediction results (Mbari, 2020).

*2.6 Spatial Pattern Change*

The distribution probability of *T. sinense* underwent reclassification, and a grid calculator was employed to delineate the distribution change layer of *T. sinense* between historical or future periods and current climate scenarios. Based on the grid values, four types of distribution area changes in *T. sinense* were redefined: retention (3), additions (2), losses (1), and non-suitable (0). The suitable area for each type was determined by calculating the proportion of each value.

## 3 Results

*3.1 Species Distribution Model and Its Accuracy*

Utilizing 232 geographic distribution data points and 36 environmental variables, we employed the MaxEnt model to simulate and predict potentially suitable areas for *T. sinense* . Optimization using the Emavel data package revealed that when the feature combination (FC) was set to LP and the regularization multiplier (RM) to 0.9, an AICc value of 0 indicated optimal predictive performance. Hence, FC = LP and RM = 0.9 were chosen as the final parameter settings (Table 2).

*3.2 Importance of Environmental Variables Affecting T. sinense Distribution*

The influence of 16 environmental factors on distribution was evaluated through a jackknife test (Fig. 2). Notably, the contribution rates (PC) of Bio6 (44.60%), T_CACO3 (10.29%), and Bio9 (8.90%) ranked highest, with a cumulative PC of 63.79%. Similarly, the permutation importance (PI) of Bio6 (34.18%), Bio4 (25.70%), and elevation (21.18%) were among the top three, with a cumulative PI of 81.06%. This analysis revealed that the primary environmental factors shaping the current geographical distribution of *T. sinense* include bioclimatic variables (Bio4 and Bio6), soil variables (T_CACO3), and topography (Elevation) (Table 3).

Environmental factor response curves further elucidated the relationship between the probability of *T. sinense* occurrence and environmental variables (Fig. 3). Generally, when the probability exceeded 0.5, corresponding environmental factor values favored *T. sinense* growth. Based on these curves, suitable environmental factor ranges for *T. sinense* growth were determined as follows: 407.4 to 731.3 (Bio4), -8 to 0.61degC (Bio6), 0% to 0.17% (T_CACO3), and 1355.8 to 3508 m (Elevation).

*3.3 Suitable Distribution Areas for T. sinense under Current Climatic Conditions*

Currently, *T. sinense* finds suitable habitat across approximately 7.24% of China's total land area. Central Sichuan, northwestern Yunnan, western Guizhou, and southwestern Hubei emerge as primary distribution hubs, with suitable areas radiating outward in distinct patterns (Fig. 4). Notably, highly suitable areas connect with moderately suitable regions, while less suitable areas extend from them. Compared to the current distribution, new suitable areas have emerged along coastal regions. Expansion of *T. sinense* distribution is observed in provinces such as Chongqing, Guizhou, and Hunan, while the species' range remains largely unchanged in other regions.

*3.4 Prediction of Suitable Areas of T. sinense in Historical and Future Climates*

This study analyzed six periods to predict potential distribution areas for *T. sinense* . Optimal distribution areas varied across periods, predominantly favoring Southwest China.

The total suitable area for *T. sinense* has exhibited fluctuations from the last interglacial period to the present (Fig. 5). Initially, it stood at 758,258 km$^2$, decreasing to 731,469.3 km$^2$, then rising to 750,132.8 km$^2$before sharply declining to 675,550.8 km$^2$. Similar trends were observed in high, medium, and low suitability areas (Table 4).

Under various climate scenarios for the 2050s and 2070s, significant changes occurred in suitable areas due to climate shifts (Fig. 5). In the 2050s, the climate scenario yielding the largest suitable area was SSPs2-4.5, which was 60,955.2 $km^2$ less than the current scenario. By 2070, SSPs1-2.6 exhibited the largest suitable area, 39,032.8 $km^2$ less than the current scenario. Across all grades, the future suitable habitat area for *T. sinense* is expected to decrease compared to the current area (Table 4).

*3.5 Changes in Spatial Pattern of Potential Suitable Areas of T. sinense*

Compared to the current period, the suitable area for *T. sinense* decreased from the last interglacial period to the mid-Holocene, followed by an increase (Fig. 6). During the mid-Holocene, an additional area of approximately 119,693.5 $km^2$ emerged, constituting 17.72% of the total area. These additions were mainly concentrated in central Yunnan and southern Gansu. Conversely, during the last glacial period, the cold climate led to a significant reduction in suitable habitats, resulting in a loss of 42,620.2 $km^2$, or a 6.3% decrease (Table 5). Losses occurred predominantly in fragmented areas at the junction of Sichuan, Yunnan, Gansu, and Shaanxi provinces. Retention areas during the Last Glacial Maximum were primarily situated in Southwest China.

The expansion rate for 2050 was lower than that for 2070 across eight different climate scenarios with similar concentrations (Fig. 6). In the 2050s, the additional area for *T. sinense* initially expanded, then contracted with increasing greenhouse gas emissions. Conversely, by the 2070s, the additional area exhibited an upward trend with increased emissions. Except for the SSPs2.6 scenario, the loss rate in the 2070s was significantly higher than that in the 2050s (Table 5). Overall, under future climate scenarios, fragmentation of potential distribution areas suitable for *T. sinense* is expected to increase. Loss areas will concentrate in the southern region of the current suitable area, while added areas will primarily occur in the north. These areas require close monitoring for potential pattern changes.

*3.6 Core Distributional Shifts*

Throughout history, the centroid of *T. sinense* has exhibited notable fluctuations (Fig. 7). From the last interglacial period to the last glacial maximum, the center of mass shifted southwest by 49,638 m. Subsequently, from the last glacial period to the mid-Holocene, the centroid moved northeast by 36,430 m. Continuing into the present era, the center of mass further migrated northeast by 18,472.6 m (Table 6).

Projection analysis indicates a northward shift in the centroid of the suitable area for *T. sinense* by 2050 and 2070, under future climate change scenarios (Fig. 7). With increasing greenhouse gas emissions, the spatial distribution of potentially suitable areas undergoes more pronounced alterations over greater distances. Notably, the migration distance of *T. sinense* in the 2070s surpasses that of the 2050s under low and medium emission concentrations, except for the center of the 2050s-SSPs8.5. The most extensive migration distance occurs under the SSPs7.0-2070s climate scenario.

## 4 Discussion

*4.1 Environmental Factors Affecting T. sinense Distribution*

Results from the jackknife test and analysis of the main parameter table underscore that the potential distribution of *T. sinense* is influenced by four key environmental factors: Bio4, Bio6, T_CACO3, and Elevation. Elevation plays a significant role in species distribution by indirectly affecting temperature and precipitation (Clark et al., 2007; Ma et al., 2021). While topsoil calcium carbonate does impose some restriction on plant distribution, its impact appears less pronounced (Wang et al., 2023). Therefore, temperature emerges as the primary factor shaping the geographical distribution of *T. sinense* , a finding corroborated by previous studies. Li (2021), for instance, employed the concept of space-time substitution to investigate the influence of altitude on the reproductive characteristics of *T. sinense* , proposing that temperature variations impact species fitness and could prompt migration to higher altitudes with rising temperatures. Similarly, Chen et al. (2023) through correlation analysis of chronological and meteorological factors, identified air temperature during specific periods as a key influencer during *T. sinense* growth stages.

The permutation importance (PI) and jackknife tests further highlight the critical role of the minimum temperature of the coldest month (bio6) in shaping the potential geographical distribution of *T. sinense* . This finding aligns with observations in other species such as *Quercus mongolica (Yin et al., 2013)* , *Santalum album (Hu et al., 2014)* , *Gymnocarpos przewalskii (Zhao et al.,2020)* , and *Thuja sutchuenensis (Ma et al., 2021)* . Chen's research also revealed a significant negative correlation between *T. sinense* growth and the lowest temperatures in November. Consequently, the minimum temperature during the coldest month emerges as a pivotal factor constraining northward expansion of *T. sinense* . Low temperatures not only hinder seed germination and morphological development but also pose challenges to the species' cold resistance, ultimately impeding its normal growth and development in northern China.

*4.2 Changes in the Potential Geographical Distribution of T. sinense*

Our investigation revealed fluctuations in the total suitable area of *T. sinense* , which decreased from 758,258 $km^2$ to 731,469.3 $km^2$ from the last interglacial period to the last glacial maximum. During this period, suitable habitat contracted, primarily concentrating in the central part of southwest China. The mountainous terrain in this region acted as a barrier against cold air, mitigating extreme climate fluctuations and providing stable conditions conducive to species survival (Stewart et al., 2010; Li, 2017). Furthermore, the absence of geographical barriers facilitated migration to this area, establishing Southwest China as a critical refuge for the Tertiary relict *T. sinense (Chen et al., 2011; Liang, 2020)* . Subsequently, from the last glacial maximum to the mid-Holocene, the total suitable area expanded to 750,132.8 $km^2$, with suitable habitat extending outward from the Sichuan Basin and Yunnan-Guizhou Plateau. This expansion correlates with the warmer and wetter global climate during the mid-Holocene, aligning with the hydrothermal conditions favorable for *T. sinense* growth. Consequently, the population of *T. sinense* exhibited significant glacial contraction and post-glacial expansion, consistent with findings for other species such as *Thuja sutchuenensis (Qin et al., 2017)* ,*Davidia involucrate (Ye et al., 2021)* , and *Ulmus elongate (Zhang et al., 2021)* .

In the future, global climate warming is anticipated to substantially impact suitable habitats for *T. sinense* , resulting in a significant distribution shift. The extent of this shift varies depending on emission scenarios, with the largest loss area observed in the SSPs8.5 scenario and the smallest in the SSPs2.6 scenario. This disparity is attributed to temperature surpassing the threshold required for optimal *T. sinense* growth in the SSPs8.5 scenario. Consequently, temperature increase emerges as a primary driver of future reductions in suitable distribution areas. Extensive research underscores the transformative effect of climate change on species distribution, often leading to migration towards higher latitudes (Thuiller, 2003; Chen et al., 2011). Consistent with this trend, our study forecasts a shift in *T. sinense* 's suitable habitats to higher latitudes under future climate scenarios. These observations suggest that previously unsuitable high-latitude regions may become conducive to *T. sinense* survival as global temperatures rise, making them preferred areas for ex situ conservation efforts. Overall, the dynamic response of *T. sinense* 's geographical distribution to climate fluctuations underscores its adaptive capacity to climate change, highlighting the necessity for strategic conservation measures.

*4.3 Protection and Management Strategy*

Our findings underscore a concerning trend: under future climate conditions, the rate of decline in *T. sinense* populations is projected to surpass the rate of expansion, posing a significant risk of extinction. Urgent action is therefore warranted to address this potential survival crisis. Identification of the primary potential distribution regions of *T. sinense* enables the strategic establishment of nature reserves in these areas, crucial for safeguarding the natural habitats of wild *T. sinense* populations.

Given the habitat loss, it is imperative to consider the impacts on associated species when devising ex situ conservation strategies. Moreover, proactive measures tailored to the growth requirements of *T. sinense* should be implemented in newly identified areas to mitigate potential disruptions. Preserving retention areas can serve as secure sanctuaries, allowing trees to adapt to climate change. Thus, it is essential to bolster the protection and management efforts in these critical zones.

## 5 Conclusions

This study employed the MaxEnt model to delineate the suitable distribution areas of *T. sinense* across different temporal periods. Our analysis identified four key environmental factors—Bio4, Bio6, T_CACO3, and Elevation—as primary determinants shaping the potential distribution of *T. sinense* . Specifically, temperature emerged as the principal factor influencing the geographical distribution of *T. sinense* .

The dynamic changes in suitable areas for *T. sinense* during historical periods adhered to the pattern of "glacial contraction and postglacial expansion." However, in the context of global warming, our findings reveal a concerning trend of decreasing suitability for *T. sinense* , with a shift towards higher-altitude regions.

These results furnish a robust scientific foundation for guiding the management, conservation, and judicious site selection strategies aimed at preserving *T. sinense* populations in the face of ongoing environmental changes.

**References**

Araujo, M. B., Peterson, A. T. Uses and misuses of bioclimatic envelope modeling. (2012). Ecology, 93(7), 1527-39. https://doi.org/10.1890/11-1930.1

Chen, D. M., Kang, H. Z., Liu, C. J. An Overview on the Potential Quaternary Glacial Refugia of Plants in China Mainland. (2011). Bulletin of Botanical Research, 31(5), 623-632.

Chen, I. C., Hill, K. J., Ohlemuller, R., Roy, B. D., Thomas, D. C. Rapid Range Shifts of Species Associated with High Levels of Climate Warming. (2011). Science, 333(6045), 1024-1026. https://doi.org/10.1126/science.1206432

Chen, R., Mao, W. L., Li, W. Y., Han, H. Y., Zhang, Xue. Mei., Gan, X. H. The photosynthetic ecophysiological adaptability of the endangered plant *Tetracentron sinense* to different habitats and altitudes. (2023). Biologia plantarum, 67, 54-66. https://doi.org/10.32615/bp.2023.005

Clark, M. J., Husband, B. C. Plasticity and Timing of Flower Closure in Response to Pollination in *Chamerion angustifolium* (Onagraceae). (2007). International Journal of Plant Sciences, 168(5), 619-625. https://doi.org/10.1086/513486

Cobos, M. E., Peterson, A. T., Barve, N., Osorio-Olvera, L. kuenm: an R package for detailed development of ecological niche models using Maxent. (2019). PeerJ, 7, e6281. https://doi.org/ 10.7717/peerj.6281

Duan, f., Li, S., Gan, X. H. Diversity analysis on leaf phenotypic traits of the endangered plant *Tetracentron sinense* . (2020). Subtropical Plant Science, 49(1), 32-40.

Elith, J., Graham, C. H., Anderson, R. P., Dudik, M., Ferrier, S., Guisan, A., Hijmans, R. J., Huettmann, F., Leathwick, J. R., Lehmann, A., Li, J., Lohmann, L. G., Loiselle, B. A., Manion, G., Moritz, C., Nakamura, M., Nakazawa, Y., Overton, J. McC., Peterson, A. T., Phillips, S. J., Richardson, K. S., Scachetti-Pereira, R., Schapire, R. E., Soberon, J., Williams, S., Wisz, M. S., Zimmermann, N. E. Novel Methods Improve Prediction of Species' Distributions from Occurrence Data. (2006). Ecography, 29(2), 129-151. https://www.jstor.org/stable/3683475

Fan, W. Q., Li, W. Y., Zhang, X. M., Gan, X. H. Photosynthetic Physiological Characteristics of *Tetracentron sinense* Oliv in Different DBH Classes and the Factors Restricting Regeneration. (2021). Journal of Plant Growth Regulation, 41(5), 1943-1952. https:// doi.org/ 10.1007/S00344-021-10421-3

Fithian, W., Elith, J., Hastie, T., Keith, D. A. Bias correction in species distribution models: pooling survey and collection data for multiple species. (2015). Methods in Ecology and Evolution, 6(4), 424-438. Htttps://doi.org/10.1111/2041-210X.12242

Fu, L. G. Plant red book in China-rare and endangered plants (Book I). Beijing: China Science Press, 452-453, 682-683.

Gao, Ya., Qin, H. Discussion on the application of MaxEnt ecologic niche model in the prediction of *Acer rubrum* introduction area. (2018). Chinese Landscape Architecture, 34(4), 89-93.

Ge, X. J., Hsu, T. W., Hung, K. H., Lin, C. J., Huang, C. C., Huang, C. C., Chiang, Y. C., Chiang, T. Y. (2012). Inferring multiple refugia and phylogeographical patterns in *Pinus massoniana* based on nucleotide sequence variation and DNA finger-printing. Plos One, 7(8), e43717. https://doi.org/10.1371/journal.pone.0043717

Graham, M. H. Confronting Multicollinearity in Ecological Multiple Regression. (2003). Ecology, 84(11), 2809-2815. https://www.jstor.org/stable/3449952

Hao, T. X., Elith, J., Lahoz-Monfort, J. J., Guillera-Arroita, G. Testing whether ensemble modelling is advantageous for maximising predictive performance of species distribution models. (2020). Ecography, 43(4), 549-558. https://doi.org/10.1111/ecog.04890

Hu, X., Wu, F. C., Guo, W., Liu, N. Identification of potential cultivation region for *Santalum album* in China by the MaxEnt ecologic niche model. (2014). Scientia Silvae Sinicae, 50(5), 27-33.

Lenoir, J., Gegout, J. C., Marquet, P. A., Ruffray, P., Brisse, H. (2008). A Significant Upward Shift in Plant Species Optimum Elevation During the 20th Century. Science, 320(5884), 1768-1771. https://doi.org/10.1126/science.1156831

Li, G. Q., Rogers, P. C., Huang, J. H. Black locust (*Robinia pseudoacacia* L.) range shifts in China: Application of a global model in climate change futures. (2021). Climate Change Ecology, 2, 100036. https://doi.org/10.1016/J.ECOCHG.2021.100036

Li, S. Study on genetic diversity of an endangered plant *Tetracentron sinense* Oliv. (2017). China west normal university.

Li, S., Gan, X. H., Han, H. Y., Zhang, X. M., Tian, Z. Q. Low within-population genetic diversity and high genetic differentiation among populations of the endangered plant *Tetracentron sinense* Oliver revealed by inter-simple sequence repeat analysis. (2018). Annals of Forest Science, 75(3), 1-11. https://doi.org/10.1007/s13595-018-0752-4

Li, Y. The effect of altitude on the reproductive characteristics of an endangered plant *Tetracentron sinense* Oliv. (2021). China west normal university.

Liang, L. Y. The influence of Quaternary glacial period on flora and vegetation in China. (2020). China Place Name, 07, 51+53.

Liu, H., Ren, H., Liu, Q., Wen X. Y., Maunder, M., Gao, J. Y. Translocation of threatened plants as a conservation measure in China. (2015). Conservation biology, 29(6), 1537-1551. https://doi.org/10.1111/cobi.12585

Lu, X. H., Xu, N., Chen, Y., Li, Y., Gan, X. H. Effects of Light Intensity and Ground Cover on Seedling Regeneration of *Tetracentron sinense* Oliv. (2020). Journal of Plant Growth Regulation, 40(2), 736-748. https://doi.org/10.1007/s00344-020-10137-w

Ma, F. Q., Guo, Q. S., Qin, A. L., Jian, Z. J., Huang, Y. J. Survival and growth of reintroduced *Thuja sutchuenensis* seedlings in relation to environmental factors. (2021). Scientia Silvae Sinicae, 57(11), 1-12.

Ma, Y. N., Lu, X. L., Li, K.W., Wang, C. Y., Guna, A., Zhang, J. Q. Prediction of Potential Geographical Distribution Patterns of *Actinidia arguta* under Different Climate Scenarios. (2021). Sustainability, 13(6), 3526. https://doi.org/10.3390/SU13063526

Ma, Y. P., Chen, G., Grumbine, R. E., Dao, Z. L., Sun, W. B., Guo, H. J. (2013). Conserving plant species with extremely small populations (PSESP) in China. Biodiversity and Conservation, 22(3), 803-809. https://doi.org/10.1007/s10531-013-0434-3

Mbari, J. N. Using species distribution models to predict the potential distribution regions of *Adansonia* in Madagascar. (2020). Chinese Academy of Sciences. https://doi.org/10.27603/d.cnki.gkhzs.2020.000021

Moreno, R., Zamora, R., Molina, J. R., Vasquez, A., Herrera, M. A. Predictive modeling of microhabitats for endemic birds in South Chilean temperate forests using Maximum entropy (Maxent). (2011). Ecological Informatics, 6(6), 364-370. http://doi.org/10.1016/j.ecoinf.2011.07.003

Pang, Y. F. Seedling raising technology of *Tetracentron sinens* e in Xiaolongshan forest area. (2018). Contemporary Horticulture, 18, 49. https://doi.org/10.14051/j.cnki.xdyy.2018.18.036

Philips, S. J., Anderson, R. P., Dudik, M., Schapire, R. E, Blair, M. E. Opening the black box: an open-source release of Maxent. (2017). Ecography, 40(7), 887-893. https://doi.org/10.1111/ecog.03049

Phillips, S. J., Dudik, M. Modeling of Species Distributions with Maxent: New Extensions and a Comprehensive Evaluation. (2008). Ecography, 31(2), 161-175. https://doi.org/10.1111/J.0906-7590.2008.5203.X

Qin, A. L., Liu, B., Guo, Q. S., Bussmann, R. W., Ma, F. Q., Jian, Z. J., Xu, G. X., Pei, S. X. Maxent modeling for predicting impacts of climate change on the potential distribution of *Thuja sutchuenensis* Franch., an extremely endangered conifer from southwestern China. (2017). Global Ecology and Conservation, 10, 139-146. https://doi.org/10.1016/j.gecco.2017.02.004

Rix, M., Crane, P. *Tetracentron sinense* : Tetracentraceae. (2007). Curtis's Botanical Magazine, 24(3), 168-173. https://doi.org/10.1111/j.1467-8748.2007.00581.x

Stewart, J. R., Lister, A. M., Barnes, L., Dalen, L. Refugia revisited: individualistic responses of species in space and time. (2010). Proceedings. Biological sciences, 277(1682), 661-671. https://doi.org/10.1098/rspb.2009.1272

Sun, Y. X., Moore, M. J., Yue, L. L., Feng, Tao., Chu, H. J., Chen, S. T., Ji, Y. H., Wang, H.C., Li, J. Q. Chloroplast phylogeography of the East Asian Arcto-Tertiary relict *Tetracentron sinense* (Trochodendraceae). (2014). Journal of Biogeography, 41(9), 1721-1732. https://doi.org/10.1111/jbi.12323

Thuiller, W. BIOMOD-optimizing predictions of species distributions and projecting potential future shifts under global change. (2003). Global Change Biology, 9(10), 1353-1362. https://doi.org/10.1046/j.1365-2486.2003.00666.x

Thuiller, W., Lavorel, S., Araujo, M. B., Sykes, M. T., Prentice, I. C. Climate change threats to plant diversity in Europe. (2005). Proceedings of the National Academy of Sciences of the United States of America, 102(23), 8245-8250. https://doi.org/10.1073/pnas.0409902102

Wang, X., Duan, F., Zhang, H., Han, H. Y., Gan, X. H. Fine-scale spatial genetic structure of the endangered plant *Tetracentron sinense* Oliv. (Trochodendraceae) in Leigong Mountain. (2023). Global Ecology and Conservation, 41, e02382. https://doi.org/10.1016/J.GECCO.2023.E02382

Wang, Y. J., Zhao, R. X., Zhou, X. Y., Zhang, X. L., Zhao, G. H., Zhang, F. G. Prediction of potential distribution areas and priority protected areas of *Agastache rugosa* based on Maxent model and Marxan model. (2023). Frontiers in Plant Science, 14, 1200796. https://doi.org/10.3389/FPLS.2023.1200796

Yang, X. Q., Kushwaha, S.P.S., Saran, S., Xu, J. C., Roy, P. S. Maxent modeling for predicting the potential distribution of medicinal plant,*Justicia adhatoda* L. in Lesser Himalayan foothills. (2013). Ecological Engineering, 51, 83-87. https://doi.org/10.1016/j.ecoleng.2012.12.004

Ye, L. Q., Zhang, W. H., Ye, X. Z., Liu, Y. P., Zhang, G. F., Liu, B., Ruan, S. N. Prediction of Potential Distribution Area and Analysis of Dominant Environmental Variables of *Davidia involucrate* Based on Maxent. (2021). Journal of Sichuan Agricultural University, 39(05), 604-612. https://doi.org/10.16036/j.issn.1000-2650.2021.05.006

Yin, X. J., Zhou, G. S., Sui, X. H., He, Q. J., Li, R. P. Potential Geographical Distribution of *Quercus wutaishanica* Forest and Its Dominant Factors. (2013). Scientia Silvae Sinicae, 49(8), 10-14.

Yu, Y. Z., Zhang, M. H., Du, H. R., Li, Q., Zhang, L. B., Mu, W. J. Optimized MAXENT model in simulating distribution of suitable habitat of moose. (2019). Journal of Northeast Forestry University, 47(10), 81-84+95. https://doi.org/10.13759/j.cnki.dlxb.2019.10.016

Zhang, H., Wang, D., Duan, F., Li, S., Gan, X. H. Construction strategy of core collection based on leaf phenotypic traits of *Tetracentron sinense* . (2019). Forest Research, 32(2), 166-173. https://doi.org/10.13275/j.cnki.lykxyj.2019.02.024

Zhang, M. Z., Ye, X. Z., Li, J. H., Liu, Y. P., Chen, S. P., Liu, B. Prediction of potential suitable area of *Ulmus elongate* in China under climate change scenarios. (2021). Chinese Journal of Ecology, 40(12), 3822-3835. https://doi.org/10.13292/j.1000-4890.202112.018

Zhao, Z. F., Wei, H. Y., Guo, Y. L., Luan, W. F., Zhao, Z. B. Impact of climate change on the suitable habitat distribution of *Gymnocarpos przewalskii* , a relict plant. (2020). Journal of Desert Research, 40(2), 125-133.

Zhuang, H. F., Zhang, Y. B., Wang, W., Ren, Y. H., Liu, F. Z., Du, J. H., Zhou, Y. Optimized hot spot analysis for probability of species distribution under different spatial scales based on MaxEnt model:*manglietia insignis* case. (2018). Biodiversity Science, 26(9), 931-940.

## Author Contributions

**Yuanjie Gan:** Conceptualization, Data curation, Methodology, Software, Writing - original draft. **Xiao -hong Gan:** Data curation, Project administration, Supervision, Visualization, Writing - review & editing. **Junfeng Tang:** Methodology, Software. **Hongyan Han:** Data curation, Software, Visualization. **Lijun Chen:** Data curation, Software, Visualization.

## Funding information

This study was supported by National Natural Science Foundation of China (No. 32070371), and the Innovation Team Funds of China West Normal University (No. KCXTD2022-4), the fund of Sichuan Meigu Dafegnding National Nature Reserve (No. mgdfd2022-13), Sichuan Micang Mountain National Nature Reserve (No. N5108212022000043), and Natural Science Foundation of Sichuan Province (No. 23NSFSC1272).

## Acknowledgements

We would like to thank Editage (www.editage.cn) for English language editing.

## Data Accessibility

Datasets used in this study are available online from the Dryad Digital Repository. (https://datadryad.org/stash/share/osQnAcuL0yh0p3g4z78YVAhXCRIoPeEDpRev5Xjc_jE).

## Tables

**Table 1 Environmental variables used in the study**

| Type | Variables | Description | UNITS |
|---|---|---|---|
| Bioclimatic variables | Bio1 | Annual Mean Temperature | |
| | Bio2 | Mean Diurnal Range | |
| | Bio3 | Isothermality | 1 |
| | Bio4 | Temperature Seasonality | 1 |
| | Bio5 | Max Temperature | |
| | Bio6 | Min Temperature of Coldest Month | |
| | Bio7 | Temperature Annual Range | |
| | Bio8 | Mean Temperature of Wettest | |
| | Bio9 | Mean Temperature of Driest Quarter | |
| | Bio10 | Mean Temperature of Warmest Quarter | |
| | Bio11 | Mean Temperature of Coldest Quarter | |
| | Bio12 | Annual Precipitation | mm |

| Type | Variables | Description | UNITS |
|---|---|---|---|
| | Bio13 | Precipitation of Wettest Month | mm |
| | Bio14 | Precipitation of Driest Month | mm |
| | Bio15 | Precipitation Seasonality | 1 |
| | Bio16 | Precipitation of Wettest Quarter | mm |
| | Bio17 | Precipitation of Driest Quarter | mm |
| | Bio18 | Precipitation of Warmest Quarter | mm |
| | Bio19 | Precipitation of Coldest Quarter | mm |
| Soil variable | T_GRAVEL | Topsoil Gravel Content | %vol. |
| | T_SAND | Topsoil Sand Fraction | % wt. |
| | T_SILT | Topsoil Silt Fraction | % wt. |
| | T_CLAY | Topsoil Clay Fraction | % wt. |
| | T_USDA_TEX_CLASS | Topsoil USDA Texture Classification | name |
| | T_REF_BULK_DENSITY | Topsoil Reference Bulk Density | kg/dm3 |
| | T_OC | Topsoil Organic Carbon | % wt. |
| | T_PH_H2O | Topsoil pH (H2O) | -log($H^+$) |
| | T-ESP | Topsoil Sodicity (ESP) | % |
| | T_CEC_CLAY | Topsoil CEC (clay) | cmol/kg |
| | T_BS | Topsoil Base Saturation | % |
| | T_TEB | Topsoil TEB | cmol/kg |
| | T_CACO3 | Topsoil Calcium Carbonate | % wt |
| | T_CASO4 | Topsoil Gypsum | % wt. |
| | T_ECE | Topsoil Salinity (Elco) | dS/m |
| | T_CEC_SOIL | Topsoil CEC (soil) | cmol/kg |
| Topography | Elev | Elevation | m |

**Table 2** Model parameter

| Model evaluation | Feature combination | Regularization multiplier | Value of delta Akaike Information criterion corrected |
|---|---|---|---|
| Default | LQHPT | 1 | 259.485332 |
| Optimized | LP | 0.9 | 0 |

**Table 3** Main parameters of environmental factors

| variable | PC | PI | RTGw | RTGo | TGw | TGo | AUCw | AUCo |
|---|---|---|---|---|---|---|---|---|
| bio6 | 44.6012 | 34.1752 | 2.1863 | 1.2083 | 2.2081 | 1.2511 | 0.9592 | 0.8887 |
| T_CACO3 | 10.2886 | 2.4837 | 2.1824 | 0.268 | 2.2161 | 0.2534 | 0.9592 | 0.6611 |
| bio9 | 8.8969 | 0.5763 | 2.1975 | 0.9028 | 2.218 | 0.9267 | 0.9595 | 0.8435 |
| Elev | 7.1365 | 21.1835 | 2.1492 | 0.6041 | 2.167 | 0.6384 | 0.9573 | 0.8059 |
| bio2 | 6.8383 | 0.036 | 2.1981 | 0.8624 | 2.2208 | 0.9352 | 0.9596 | 0.8285 |
| bio10 | 5.0883 | 0.0595 | 2.1982 | 0.3042 | 2.2196 | 0.3437 | 0.9595 | 0.723 |
| T_GRAVEL | 3.4221 | 0.1516 | 2.1925 | 0.1493 | 2.2205 | 0.1051 | 0.9597 | 0.6468 |
| bio7 | 3.0458 | 0.1643 | 2.1981 | 1.1432 | 2.218 | 1.2907 | 0.9595 | 0.8902 |
| bio4 | 2.9022 | 25.6958 | 2.1867 | 0.9363 | 2.2065 | 1.0171 | 0.9592 | 0.8546 |
| T_SILT | 2.288 | 1.5817 | 2.1681 | 0.3146 | 2.1914 | 0.352 | 0.9581 | 0.7978 |
| bio5 | 1.4892 | 0.0014 | 2.1982 | 0.4146 | 2.2185 | 0.4884 | 0.9595 | 0.7767 |
| bio15 | 1.2819 | 1.5014 | 2.1853 | 0.5794 | 2.2109 | 0.6629 | 0.9595 | 0.7961 |
| bio3 | 1.1263 | 6.6682 | 2.1787 | 0.031 | 2.2096 | 0.0282 | 0.9593 | 0.5629 |

| variable | PC | PI | RTGw | RTGo | TGw | TGo | AUCw | AUCo |
|---|---|---|---|---|---|---|---|---|
| T_BS | 0.7965 | 0.1273 | 2.1921 | 0.025 | 2.216 | 0.0211 | 0.9595 | 0.599 |
| bio19 | 0.5863 | 3.4403 | 2.1792 | 0.6257 | 2.1864 | 0.7266 | 0.9581 | 0.8264 |
| bio17 | 0.2119 | 2.1538 | 2.1901 | 0.535 | 2.2044 | 0.6404 | 0.9589 | 0.8139 |

**Table 4 Potential suitable area(km$^2$) of*T. sinense* in different periods in China**

| Climate change scenario | Highly suitable | Moderately suitable | Low suitable | Not suitable | Total suitable |
|---|---|---|---|---|---|
| Last interglacial | 220609 | 245260 | 292389 | 8568151.7 | 758258 |
| Last glacial maximum | 217999.5 | 239164.6 | 274305.2 | 8594941 | 731469.3 |
| Middle Holocene | 203313.5 | 251405 | 295414.4 | 8576277 | 750132.8 |
| Current | 195840.9 | 206532.9 | 273177 | 8650859 | 675550.8 |
| 50s-126 | 162704 | 176595 | 247549.9 | 8739560.9 | 586849.1 |
| 50s-245 | 192927.2 | 176594.6 | 245073.8 | 8711814.3 | 614595.6 |
| 50s-370 | 170920.9 | 171981.6 | 235157 | 8748350 | 578059.7 |
| 50s-585 | 140107 | 153678 | 225895.6 | 8806728.9 | 519681.1 |
| 70s-126 | 184676.7 | 190283.7 | 261558 | 8689891 | 636518 |
| 70s-245 | 186343.6 | 181006.1 | 262349.4 | 8696710.9 | 629699.1 |
| 70s-370 | 126653.7 | 145377 | 238204 | 8816175 | 510235 |
| 70s-585 | 172671.4 | 174607.7 | 244501 | 8734629 | 591780 |

**Table 5 Spatial changes of suitable areas of *T. sinense*under different climate change scenarios**

| Period | Area/km$^2$ | Area change rate/% | | | | | | |
|---|---|---|---|---|---|---|---|---|
| | Addition | Loss | Retention | Change | Increasing rate | Attrition rate | Retention rate | Tot |
| LIG | 111055 | 28374.16 | 647234 | 82680.79 | 16.44 | 4.20 | 95.81 | 108 |
| LGM | 98509.7 | 42620.18 | 632988 | 55889.52 | 14.58 | 6.31 | 93.70 | 101 |
| MID | 119693.5 | 29653.95 | 645954.2 | 90039.55 | 17.72 | 4.39 | 95.62 | 108 |
| 50s-126 | 32884.35 | 121586.2 | 553949 | -88701.9 | 4.87 | 18.00 | 82.00 | 68.8 |
| 50s-245 | 77403.53 | 138390.2 | 537160.6 | -60986.6 | 11.46 | 20.49 | 79.51 | 70.4 |
| 50s-370 | 61542.51 | 159033.9 | 516485.6 | -97491.4 | 9.11 | 23.54 | 76.45 | 62.0 |
| 50s-585 | 47145.94 | 203047.5 | 472503.4 | -155902 | 6.98 | 30.06 | 69.94 | 46.8 |
| 70s-126 | 48964.43 | 88028.21 | 587522.6 | -39063.8 | 7.25 | 13.03 | 86.97 | 81.1 |
| 70s-245 | 99629.48 | 145428.4 | 530038.2 | -45798.9 | 14.75 | 21.53 | 78.46 | 71.0 |
| 70s-370 | 78531.53 | 243828.3 | 431704.5 | -165297 | 11.62 | 36.09 | 63.90 | 39.4 |
| 70s-585 | 113049.2 | 196851.1 | 478699.7 | -83801.9 | 16.73 | 29.14 | 70.86 | 58.4 |

**Table 6 Migration distance of geometric center (centroid) in different periods (m)**

| Period | LIG | LGM | MID | Current | 50s-126 | 50s-245 | 50s-370 | 50s-585 | 70s-126 | 70s-245 |
|---|---|---|---|---|---|---|---|---|---|---|
| LGM | 33950.5 | | | | | | | | | |
| MID | 4972 | 36430 | | | | | | | | |
| Current | 20133.09 | 49638 | 18472.63 | | | | | | | |
| 50s-126 | 73582.7 | 65988.3 | 78570 | 79712 | | | | | | |
| 50s-245 | 123114.49 | 111802.1 | 127703.3 | 129707.41 | 5014.1 | | | | | |
| 50s-370 | 130270 | 65062.36 | 134714.8 | 134823.7 | 57059.5 | 6885.6 | | | | |

| Period | LIG | LGM | MID | Current | 50s-126 | 50s-245 | 50s-370 | 50s-585 | 70s-126 | 70s-245 |
|---|---|---|---|---|---|---|---|---|---|---|
| 50s-585 | 55544.1 | 86973.2 | 55554.5 | 38454.9 | 95552.1 | 140294.9 | 145801.3 | | | |
| 70s-126 | 76448.8 | 727891.1 | 84055.07 | 78898.7 | 13110.8 | 51777 | 57645.9 | 90884.8 | | |
| 70s-245 | 171502.3 | 149463.6 | 175706.1 | 181600.77 | 106209.6 | 66674 | 64404.9 | 200991.97 | 112911.7 | |
| 70s-370 | 186607.7 | 176207 | 191284 | 189485 | 113422 | 65714.1 | 59129.5 | 194819 | 112498.6 | 76737.4 |
| 70s-585 | 175217.87 | 159380.6 | 179049 | 181371 | 102275 | 52709 | 46801 | 192843 | 103796 | 44940 |

**Legends, and labeling**

Figure 1. Distribution points of *T. sinense* after data cleaning.

Figure 2. The jackknife test result for the environmental factors.

Figure 3. Response curves of dominant environmental factors.

Figure 4. Suitable distribution of *T. sinense* in China under current climatic conditions.

Figure 5. Prediction of potential suitable areas of *T. sinense* in different period.

Note: LIG, Last interglacial; LGM, Last glacial maximum, MID: Mid Holocene; 50s-126˜50s-585 were SSPs1-2.6, SSPs2-4.5, SSPs3-7.0 and SSPs5-8.5 of 2050s, respectively; 70s-126˜70s-585 were SSPs1-2.6, SSPs2-4.5, SSPs3-7.0 and SSPs5-8.5 of 2070s, respectively. The same as below.

Figure 6. Spatial pattern changes of T. sinense under different climate change scenarios.

Figure 7. The core distributional shifts of suitable habitat under different climate scenario for *T. sinense* .

**Hosted file**

`Figure_1.tiff` available at https://authorea.com/users/810278/articles/1211651-evaluating-the-vulnerability-of-tetracentron-sinense-habitats-to-climate-induced-altitudinal-shifts

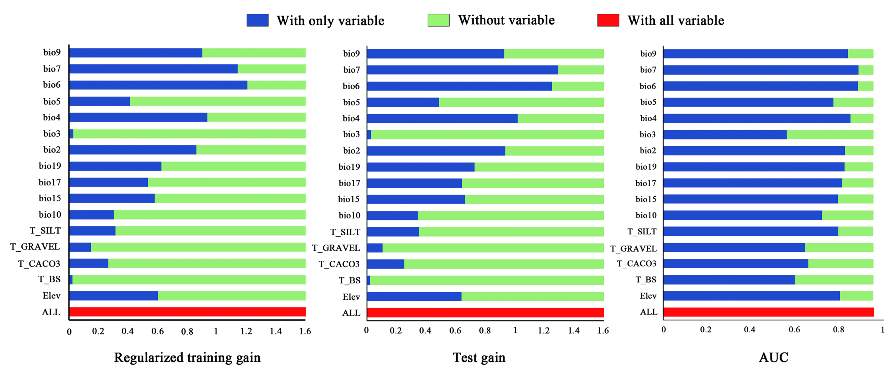


**Hosted file**

`Figure_3.tiff` available at https://authorea.com/users/810278/articles/1211651-evaluating-the-vulnerability-of-tetracentron-sinense-habitats-to-climate-induced-altitudinal-shifts

**Hosted file**

`Figure_4.tiff` available at https://authorea.com/users/810278/articles/1211651-evaluating-the-vulnerability-of-tetracentron-sinense-habitats-to-climate-induced-altitudinal-shifts

**Hosted file**

Figure_5.tiff available at https://authorea.com/users/810278/articles/1211651-evaluating-the-vulnerability-of-tetracentron-sinense-habitats-to-climate-induced-altitudinal-shifts

**Hosted file**

Figure_6.tiff available at https://authorea.com/users/810278/articles/1211651-evaluating-the-vulnerability-of-tetracentron-sinense-habitats-to-climate-induced-altitudinal-shifts

**Hosted file**

Figure_7.tiff available at https://authorea.com/users/810278/articles/1211651-evaluating-the-vulnerability-of-tetracentron-sinense-habitats-to-climate-induced-altitudinal-shifts